LARGE EDDY SIMULATION OF TURBULENT COMBUSTION

Principle Investigator:
Heinz Pitsch
Flow Physics and Computation
Department of Mechanical Engineering
Stanford University
Stanford, CA 94305-3030

Grant number: F49620-03-1-0258

Final Performance Report
Reporting period: 10/01/2002–10/01/2005

Report Documentation Page

Form Approved
OMB No. 0704-0188

1. REPORT DATE	2. REPORT TYPE	3. DATES COVERED
15 MAR 2006	**N/A**	**-**

4. TITLE AND SUBTITLE	5a. CONTRACT NUMBER
Large Eddy Simulation of Turbulent Combustion	5b. GRANT NUMBER
	5c. PROGRAM ELEMENT NUMBER
6. AUTHOR(S)	5d. PROJECT NUMBER
	5e. TASK NUMBER
	5f. WORK UNIT NUMBER
7. PERFORMING ORGANIZATION NAME(S) AND ADDRESS(ES) **Leland Stanford Junior University 651 Serra Street Stanford, CA 94305**	8. PERFORMING ORGANIZATION REPORT NUMBER
9. SPONSORING/MONITORING AGENCY NAME(S) AND ADDRESS(ES)	10. SPONSOR/MONITOR'S ACRONYM(S)
	11. SPONSOR/MONITOR'S REPORT NUMBER(S)

12. DISTRIBUTION/AVAILABILITY STATEMENT
Approved for public release, distribution unlimited

13. SUPPLEMENTARY NOTES
The original document contains color images.

14. ABSTRACT

15. SUBJECT TERMS

16. SECURITY CLASSIFICATION OF:			17. LIMITATION OF ABSTRACT	18. NUMBER OF PAGES	19a. NAME OF RESPONSIBLE PERSON
a. REPORT	b. ABSTRACT	c. THIS PAGE			
unclassified	**unclassified**	**unclassified**	**SAR**	**32**	

1 Sub-Grid Models for Large Eddy Simulation of Turbulent Combustion

1.1 Introduction

In the past decade, Large Eddy Simulation (LES) has been increasingly and successfully applied to both premixed and non-premixed reacting flows [1, 2, 3]. In application and testing, methods such as steady and unsteady flamelet modeling, the probability density function (PDF) assumption, and level set tracking have been shown to describe combustion in a LES context correctly. As capable as such methods are, however, researchers only very recently have begun to apply them to the detailed, multi-scale, and multi-physics flows that arise in the burners and engines found in modern, industrially relevant equipment. In the course of this transition of LES from a scientifically interesting method in its own right to a research platform useful for studying real world flows, the limits of current methods to be highlighted.

More specifically, as the complexity of the flows being considered increases, so do the number of involved lengthscales, the details of the relevant chemistry, and the extent of the turbulence-chemistry interactions. In LES, where the large scales of the flow are resolved while the small scales are modeled, this increased complexity means that more accuracy will be demanded of sub-grid models. Sub-grid models for momentum have been studied rigorously, and computationally efficient methods exist. But sub-grid models for combustion-related phenomena have not yet demonstrated the ability to capture the physics needed to describe complex flows consistently and accurately. For example, quantities of interest such as flame lift-off heights and heat release near injection nozzles, often are predicted incorrectly using state-of-the-art codes. Furthermore, NO_x and soot formation processes, which occur on timescales significantly longer than those of CO_2 and H_2O production, cannot be captured with the kind of steady flamelet models now being used [4].

Part I of this project was proposed in response to these challenges. The goal of part I has been, broadly, to improve the predictive capability of LES of turbulent reacting flows. To meet this challenge, more specific goals were set for each of the three combustion regimes of industrial interest: non-premixed, premixed, and partially-premixed flows.

In non-premixed flows, fuel and oxidizer enter a combustion chamber separately. These components are combined by mixing processes to sustain chemical reactions within the chamber. In turbulent flows where small eddies can influence mixing processes strongly, sub-grid scale models for the mixture fraction must be accurate and robust. The goal of the non-premixed portion of this project was to assess and improve models for the scalar variance and to test the limitations of these models when used in complex flame simulations.

In premixed flows, reactions most often occur in thin flame fronts. These reactions induce front propagation, a phenomenon described by the burning velocity. The burning velocity is a scalar quantity that must describe the effects of chemistry as a function of flow conditions. In turbulent flames, where eddies can influence the propagation of the front, the burning velocity also must describe the effects of turbulence on front propagation. Thus, accurately modeling

this quantity is of crucial importance. The second goal of part I, then, was the development of a new method of describing front propagation in premixed turbulent flows. This method should be able to account for variations of local equivalence ratio, the amount of unresolved local turbulence, and the local resolution of the numerical flame front solution.

Finally, in partially-premixed flows, chemical reactions can occur in both of the modes described above. Regions where fuel and oxidizer have mixed but not ignited may exist locally within the flow, such as in strong recirculation zones or in the pre-burn region of lifted flames. Conversely, purely diffusive burning may occur in regions of strong shear where fuel and oxidizer streams interact. Such flames recently have received the attention of many researchers [5, 6], but, in order to perform accurate simulations, aspects of both premixed and non-premixed models must be used. With this motivation, the last goal of part I was to validate and augment a Combined Conserved Scalar/Level Set Flamelet approach based on a multi-flamelet model.

In the following sections, the methods developed to meet these goals will be described, and the results of the simulations performed to test them will be shown. A concluding section which summarizes the entire project will follow the presentation of part II of the report.

1.2 Non-Premixed Turbulent Combustion

Reactions in non-premixed combustion in technical systems most often are limited by the processes that mix fuel and oxidizer. While macroscopic structures such as large-scale vorticies can force some of this mixing, small-scale mixing is required to achieve maximum heat release rates. This requirement exists because only when molecular mixing occurs do the maximum number of reactant molecules come into contact with each other. The mixture fraction variable, Z, is a conserved scalar quantity used to describe this mixing between fuel and oxidizer streams. Thus, an appropriate description of the sub-filter mixture fraction distribution is critical for predictive LES. Normally, the statistical moments of the conserved scalar, namely the resolved scalar and the sub-filter variance, are used to obtain a PDF-based description of the sub-filter structure. Treatment of the resolved scalar with a transport equation is straightforward, but treatment of the variance is problematic.

Although several models for the sub-filter variance exist in the literature [7, 8, 9], none are able to describe the sub-filter structure adequately. Existing models rely on the so-called local equilibrium assumption that equates the production of the sub-filter variance to the dissipation. In turbulent flows, such an equilibrium cannot be satisfied instantaneously, but only in an average sense. In spite of this drawback, the dynamic model, which makes use of this assumption, is one of the most commonly used sub-filter variance models. Adding to the problem, the numerical implementation of this model involves the additional ad-hoc assumption of directional averaging, which is required to remove certain singularities. So far, no convincing physical explanation has been provided for such an averaging procedure. A final difficulty in correctly describing the mixture fraction field is the filter size itself. Pope pointed out that LES is an incomplete model if the filter size can be arbitrarily specified [10]. In this case, arbitrary specification negates the possibility of setting limits on the requirements for a sub-filter variance model.

Work performed under this project has led to two major accomplishments that address these issues. The first is the development of a new method for describing the sub-filter variance of Z. The second is a recursive filter refinement (RFR) procedure designed to overcome the arbitrary nature of filter specification.

The dynamic modeling (DM) procedure for the sub-filter variance mentioned above was proposed by Pierce and Moin [8]. Based on the assumption of local equilibrium, and using a modeled dissipation rate, the variance model can be written as

$$\overline{Z"^2} = C\Delta^2(\nabla\overline{Z})^2\,, \tag{1}$$

where Δ is the filter width and C is a coefficient to be determined. The dynamic modeling procedure is then given by

$$\widehat{\overline{Z}\overline{Z}} - \widehat{\overline{Z}}\widehat{\overline{Z}} = C\widehat{\Delta}^2(\nabla\widehat{\overline{Z}})^2 - C\widehat{\Delta^2(\nabla\overline{Z})^2}\,, \tag{2}$$

where $\widehat{\cdot}$ denotes test filtering. This equation is solved by making the assumption that $\widehat{C} = C$, and using a least squares estimation technique.

To overcome the aforementioned drawbacks of this procedure, a new method has been developed. This method is based on the solution of a transport equation for the second moment of the mixture fraction, ($\overline{Z^2}$). This transport equation does not contain any production terms, but does contain the scalar dissipation rate, which is modeled using

$$\overline{\chi} = \frac{C_z}{\tau}\left(\overline{Z^2} - \overline{Z}^2\right)\,, \tag{3}$$

where C_z is a dynamically determined coefficient and τ is a suitable turbulent time-scale. With the solution to the transport equation

$$\frac{\partial\overline{Z^2}}{\partial t} + \nabla\cdot\left(\overline{\mathbf{u}}\overline{Z^2}\right) = \nabla\cdot\left(\alpha\nabla\overline{Z^2}\right) + \nabla\cdot\left(\overline{\mathbf{u}}\overline{Z^2} - \overline{\mathbf{u}Z^2}\right) - \left(2\alpha\left(\nabla\overline{Z}\right)^2 + \overline{\chi}\right), \tag{4}$$

the sub-filter variance can be obtained as

$$\overline{Z"^2} = \overline{Z^2} - \overline{Z}^2. \tag{5}$$

Unfortunately, typical dynamic modeling procedures assume azimuthal homogeneity and scale independence of the modeled coefficient (C_z in Eq. 3). To overcome this issue, the dynamic localization (DL) procedure is used to formulate an integral equation that then is solved using an iterative technique to obtain C_z as a three-dimensional field. This dynamic modeling procedure was developed assuming local equilibrium and tested using DNS, as well as LES simulations. Results from shear-flow calculations, shown in Figure 1, indicate that the dynamic model over-predicts the scalar-to-mechanical time-scale ratio compared to the DL model by a factor of 10. The DL model consequently predicts a higher variance across the shear-layer.

The second accomplishment in this part of the program was the development of the recursive filter refinement (RFR) method [11]. In this method, the ratio of the sub-filter scalar variance

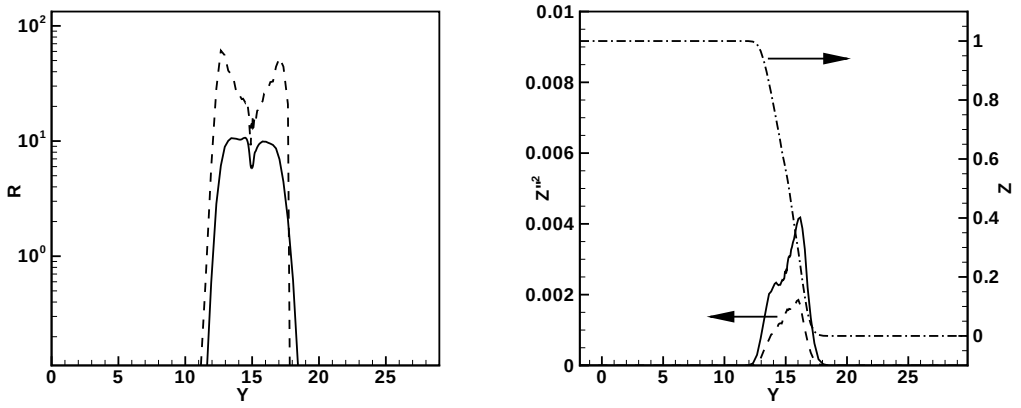

Figure 1: (Left) Comparison of scalar-to-mechanical time-scale ratios R computed using DM (dashed) and DL (solid) procedures. (Right) Comparison of variance $\overline{Z"^2}$ computed using DM (dashed) and DM (solid) models.

to the maximum possible variance is evaluated and used to describe the local resolution of the mixture fraction field. Since the maximum local variance based on the resolved mixture fraction is $\overline{Z}$(1-$\overline{Z}$), this parameter may be written

$$\alpha = \frac{\overline{Z"^2}}{\overline{Z}(1-\overline{Z})}. \tag{6}$$

When α is high, the mixture fraction field is not well resolved, and a large demand is placed on the sub-grid model. When α is low, a certain level of field resolution is guaranteed, and the importance of the model drops. In practice, this procedure is used to determine the distribution of the filter-size that is suited to a particular flow. The distribution of α can be evaluated from an instantaneous LES solution. Everywhere in the flow domain where α is above a certain tolerance, the mesh is refined in order to guarantee the effectiveness of the sub-grid model.

We have demonstrated in the simulation of a bluff-body stabilized flame, which was experimentally studied by Dally et al. [12], that the application of the RFR method significantly improves the results [11]. All velocity components, scalar and temperature profiles predicted by the simulation were in very good agreement with experimental values. Examples of temperature and carbon monoxide results are compared with experimental data in Figs. 2 and 3.

To illustrate the complex unsteady fluid dynamics in the system, a ray-tracing based visualization of the flame is shown in Figure 4. It is clear that a temporally accurate and spatially well-resolved simulation is essential for predicting such complex flame configurations.

1.3 Premixed Turbulent Combustion

Because reactions in premixed flows occur in thin fronts, level sets have been suggested as means of modeling premixed combustion [13]. Level sets describe iso-contours of field variables. They

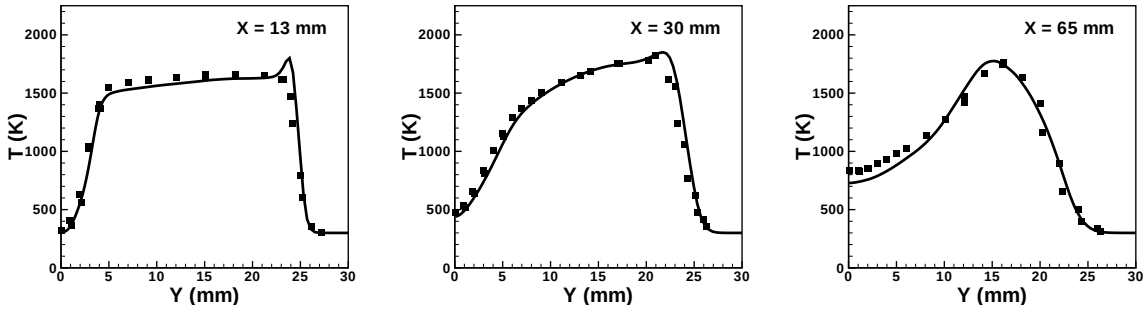

Figure 2: Radial profiles of time-averaged temperature (solid lines) compared with experimental data (symbols) at axial locations of X = 13, 30, and 65 mm.

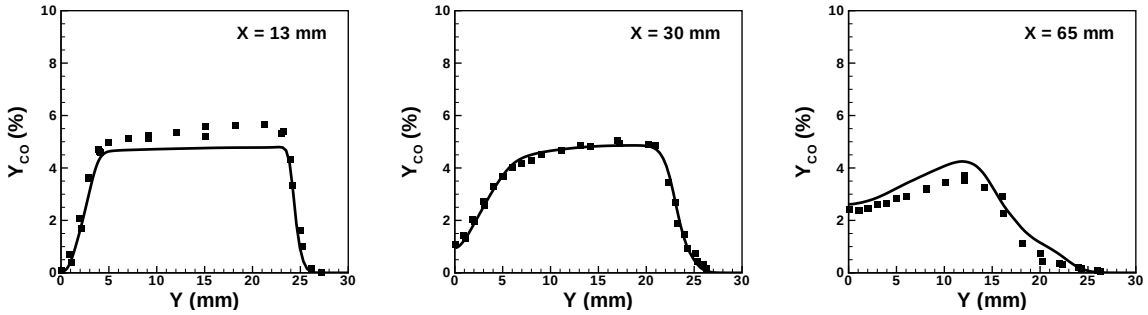

Figure 3: Radial profiles of time-averaged CO mass fraction (solid lines) compared with experimental data (symbols) at axial locations of X = 13, 30, and 65 mm.

are governed by a transport equation valid at the iso-contour of interest and a reinitialization procedure that sets the field variable away from the iso-contour. For premixed reacting flows, the so-called G-equation typically is used to describe the flame front. This equation differs from a simple advection equation only in that it contains a source term describing front propagation.

Since the inception of level set-based models, a number of issues have limited their application to LES. The first such issue is the representation of the burning velocity. To describe a variety of industrially relevant flames, this parameter functionally must depend on local quantities such as the equivalence ratio, pressure, temperature, and turbulence. A second issue is filtering. Because the level set transport equation is valid only at a two-dimensional surface in the three-dimensional space, volumetric filtering procedures cannot be applied.

In meeting the goals of the premixed section of this project, a new filtering procedure for level sets was developed successfully. That procedure led, in turn, to a new model for the turbulent burning velocity. Finally, based on simulations performed using this model, a new sensitivity in premixed combustion simulations has been identified as an area in which additional work could improve the accuracy of these types of simulations greatly.

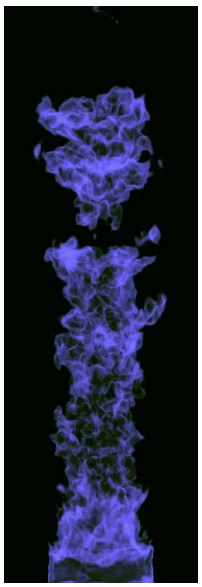

Figure 4: Visualization of the bluff-body stabilized flame using a ray-tracing technique.

The filtering procedure developed for the G-equation [14] first 'filters' the level set variable itself by integrating it over a computational cell volume as the argument of a Heaviside function

$$\check{G}(\mathbf{x},t) = \int_V H(G(\mathbf{x}-\mathbf{r},t))d\mathbf{r}. \tag{7}$$

The Heaviside function separates the flow in two regions with temperatures below and above the inner layer temperature. The filtered field then is an average over these regions. Using this new variable, a filtered transport equation may be derived as

$$\frac{\partial \check{G}}{\partial t} + \widehat{\boldsymbol{v}}_u \cdot \nabla \check{G} = s_{T,u} \left|\nabla \check{G}\right| . \tag{8}$$

This equation has two unclosed terms: the convection velocity $\widehat{\boldsymbol{v}}_u$ and the burning velocity $s_{T,u}$. The convection velocity appearing in this equation is an average conditioned on the location of the flame surface. To relate $\widehat{\boldsymbol{v}}_u$ to the unconditionally Favre-filtered velocity, $\widetilde{\boldsymbol{v}}$, which is known from the solution of the momentum equations, an additional model was developed. Applying this model results in the following equation, which governs the filtered flame front location

$$\frac{\partial \check{G}}{\partial t} + \widetilde{\boldsymbol{v}} \cdot \nabla \check{G} = \frac{\rho_u}{\overline{\rho}} s_{T,u} \left|\nabla \check{G}\right| . \tag{9}$$

While standard filtering procedures for LES do not, in and of themselves, introduce errors into the equations being solved, that is not the case here. The need to model the convective velocity used in the filtered level set equation introduces an error prior to numerical solution. It can be shown, however, that this error is proportional to some power of the filter size being used,

and thus, in most cases, it is negligible. Hence, this new filtering procedure is a significant result.

Interestingly, because of this new procedure, a propagation term proportional to the curvature of the mean front, which appeared in earlier formulations of the filtered G-equation, is no longer present in Eq. (9). This difference is important because the curvature term has a stabilizing effect on the flame front and can, therefore, lead to a reduction in resolved flame wrinkling. In the filtered equation, this effect instead must be captured by the model for the turbulent burning velocity, the second unclosed term.

A model for the turbulent burning velocity that includes this stabilizing effect has been developed under this project [14]. In this model, the front propagation velocity is described using 4 terms as

$$s_{T,u} = (s_L + s_T - D\check{\kappa} - D_t\check{\kappa}) \tag{10}$$

which account for, respectively, the resolved laminar propagation speed s_L, the resolved turbulence induced propagation s_T, the sub-filter turbulent contribution $D\check{\kappa}$, and the interaction of resolved curvature and sub-filter mixing $D_t\check{\kappa}$. Here, D is the diffusivity, D_t the turbulent diffusivity, and $\check{\kappa}$ the resolved curvature.

For completeness, s_T in Eq. (10) is developed further through an equation describing the magnitude of the length scale separating the filtered flame front location from the exact front location. The production and dissipation terms in this equation are assumed to be in balance, yielding the analytic expression

$$\frac{s_T}{s_L} = -\frac{\nu_t s_L}{4\mathrm{Sc}_t D v'_\Delta} + \sqrt{\left(\frac{\nu_t s_L}{4\mathrm{Sc}_t D v'_\Delta}\right) + \frac{\nu_t}{\mathrm{Sc}_t D}}\,, \tag{11}$$

where ν_t is the turbulent viscosity, Sc_t the turbulent Schmidt number, and v'_Δ the sub-grid scale velocity.

These models have been tested in simulations of the premixed turbulent Bunsen flames experimentally studied by Chen [15]. The results of these tests are shown in Figs. 5 and 6.

Figure 6 shows statistically averaged species and axial velocity results. Species such as H_2O and CO_2 are in excellent agreement with experimental values. Additionally, only very small discrepancies exist in the axial velocity plots. These results demonstrate the capabilities of these newly developed premixed models.

Figure 7 shows data from similar simulations is run using the filtering and burning velocity model developed here, but with a different, supposedly more accurate, heat release model. In this case, the transition from unburned to burned gas occurs too rapidly, and the slopes of the species plots are too steep near the flame front. These results indicate that there is more work to be done in this area. Although an appropriate filtering procedure and propagation model have been developed for level set based methods in LES, complete confidence in predictions is not yet possible. Specifically, the simulations run under this project have demonstrated the importance of the models describing heat release around the flame front, which need to be investigated further.

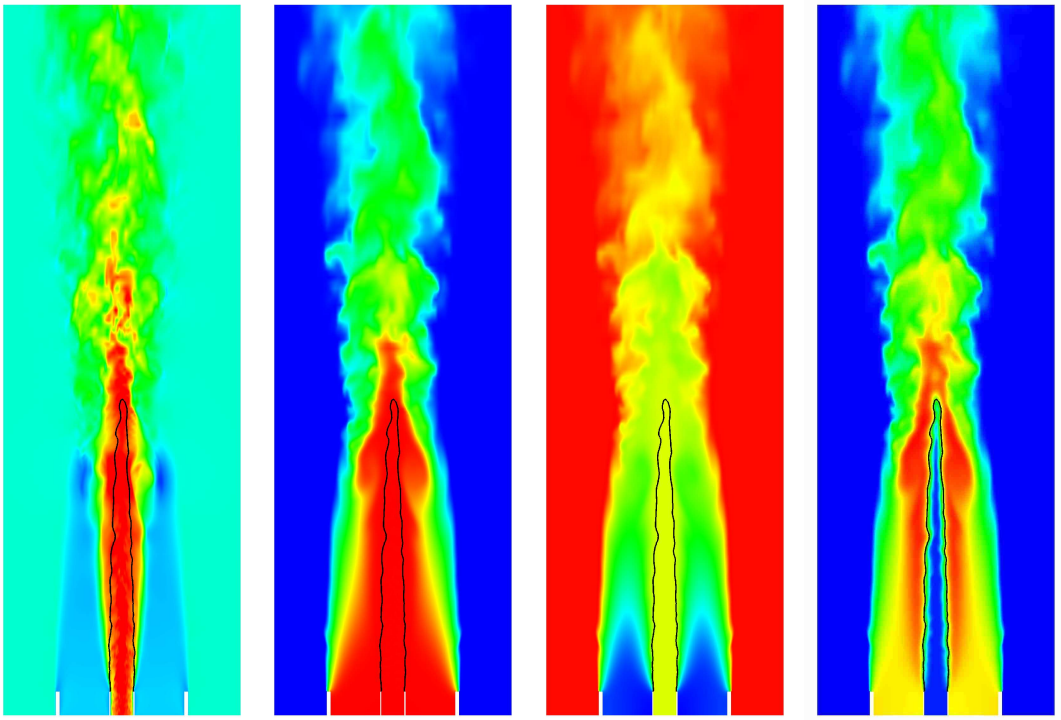

Figure 5: Contour plots of F3 premixed flame simulation. The black line represents the flame front. With red denoting high and blue denoting low values, the quantities and ranges shown are, from left to right: (a) Axial Velocity $[-7.5, 37.5]\ \frac{\text{m}}{\text{s}}$ (b) Mixture Fraction $[0, 1]$ (c) Total Enthalpy $[-1200, -200]\ \frac{\text{J}}{\text{mol}}$ (d) Temperature $[300, 2100]$ K.

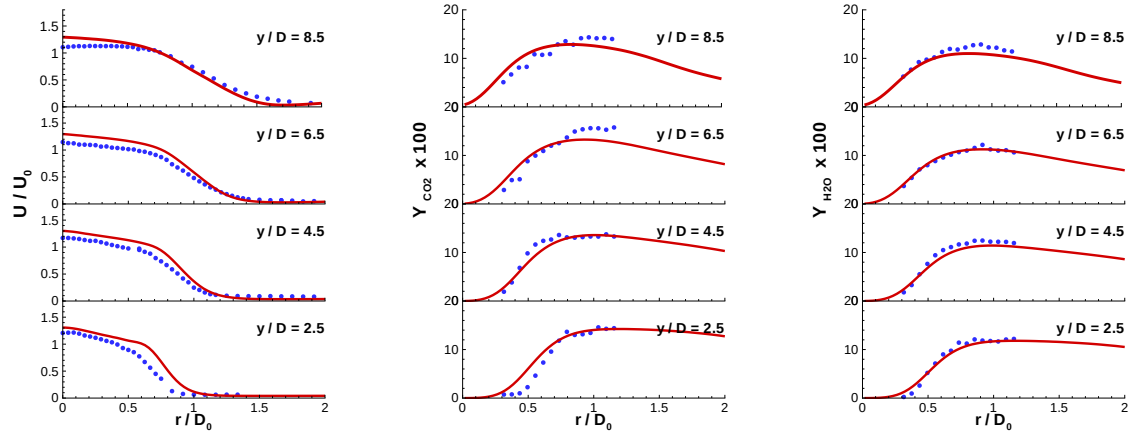

Figure 6: Radial profiles of time-averaged axial velocity, CO_2 mass fraction, and H_2O mass fraction from F3 premixed flame simulation. Combustion effects around the front are captured accurately.

1.4 Partially-Premixed Turbulent Combustion

In many technical combustion applications, pure non-premixed or premixed combustion modes may not be valid, and partially premixed combustion must be considered. For example, in the

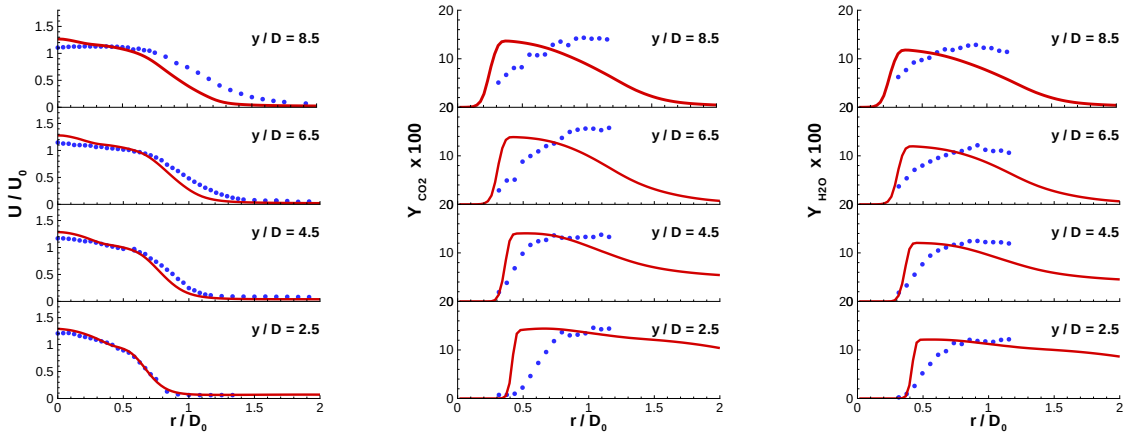

Figure 7: Radial profiles of time-averaged axial velocity, CO_2 mass fraction, and H_2O mass fraction from F3 premixed flame simulation. Here, combustion effects around the front are not accurately modeled.

stabilization region of a lifted non-premixed flame, fuel and oxidizer have time to mix before reacting, and front-like behavior develops. To describe such situations, a Combined Conserved Scalar/Level Set Flamelet model, in which both premixed and non-premixed combustion modes are considered, has been proposed [16, 17]. In this formulation, a level set method is used to describe partially premixed flame propagation and to distinguish between burned and unburned regions. The reacting gases in the post-flame region are then described by a laminar diffusion flamelet approach.

In the initial phase of this work, directed toward model validation, two areas in which this formulation suffered were identified. The first area involved how flamelet models, which typically had been considered in non-premixed contexts, should be expressed near flame fronts. The second area was the reliance of the method on a flamelet formulation for density, which would not be valid on the unburned side of the flame front where preheating occurs. Since similar issues were encountered in premixed modeling, a level set formulation was used as a starting point, with the goal of formulating solutions valid in both premixed and partially-premixed regimes.

First, a new method for computing the filtered density was devised. In this method, the density is determined directly from the temperature, for which a transport equation is solved. This temperature equation is to be solved only in the unburned region. The burned gas temperature, determined from the steady flamelet library, is enforced through a source term as a boundary condition at the flame front. The flame position is still determined from the G-equation and then imposed on the temperature equation. It would be incorrect to solve only a temperature equation in numerical computations of premixed turbulent combustion. This model proved to be very successful and was used in the premixed computations described in section 1.3.

Second, a description of a flamelet model valid near flame fronts was developed. In this model, a PDF describing the likelihood of finding burned gas around the flame front is presumed. This PDF is Gaussian in shape, with the mean set by the local value of the filtered level set

variable. This PDF can be used to compute the temperature equation source term, but more generally, the filtered value of any reactive quantity $\widetilde{\phi}$ may be computed as

$$\widetilde{\phi} = \phi_b \int_{-\infty}^{0} P(G)dG + \phi_u \int_{0}^{\infty} P(G)dG = \phi_b p_b + \phi_u p_u \,, \tag{12}$$

where $P(G)$ is the PDF and subscripts b and u denote burned and unburned values, respectively. As an example of how this equation is applied, consider a flamelet model that presumes functional dependencies on mixture fraction, Z, and total enthalpy, H. Given the joint PDF's describing those dependencies, a filtered quantity conditioned on the flame front can be written as

$$\widetilde{\phi}\left(\widetilde{G}, \widetilde{Z}, \widetilde{H}\right) = p_b \iint \phi_b(Z,H)P(Z,H)dZdH + p_u \iint \phi_u(Z,H)P(Z,H)dZdH \,, \tag{13}$$

where the burned and unburned values of the scalar are computed using the presumed PDF describing reactions around the flame front. Because of the success of this formulation, it was used with slight modifications to compute species concentrations in the premixed Bunsen flame described in section 1.3. Those results indicated that such a model works very well when the PDF describing reactions around the flame front is correct.

These new methods were applied within the Combined Conserved Scalar/Level Set Flamelet Model, which was tested through simulations of a partially-premixed case. Specifically, the experiment by Spadaccini et al. [18], a well documented gas-phase dump combustor, was used. This experiment mimics a simplified aircraft engine combustor where fuel and air enter the combustion chamber separately, but the flame lifts off from the nozzle and is stabilized through multiple recirculation regions.

Figure 8 shows contour plots from this simulation. These figures show the diffusive nature of the burning in most of the flame. Without the indicated level set, however, predicting the flame lift-off is very difficult. Figure 9 shows predicted CO mass fractions at two different cross-sections in the combustor compared with experimental data. Although for overall lean combustion CO mass fractions are very sensitive to flow conditions, experimental data are matched well.

In summary, the Combined Conserved Scalar/Level Set Flamelet Model has been demonstrated to be successful in simulating partially-premixed combustion. As might be expected, however, it suffers from the same sensitivities to the PDF describing the flame front that premixed formulations do. More rigorously, this sensitivity is a dependence on the length scale associated with the PDF in Eq. 12. With further development of the methods used to describe this length scale, partially-premixed simulations will become only more accurate.

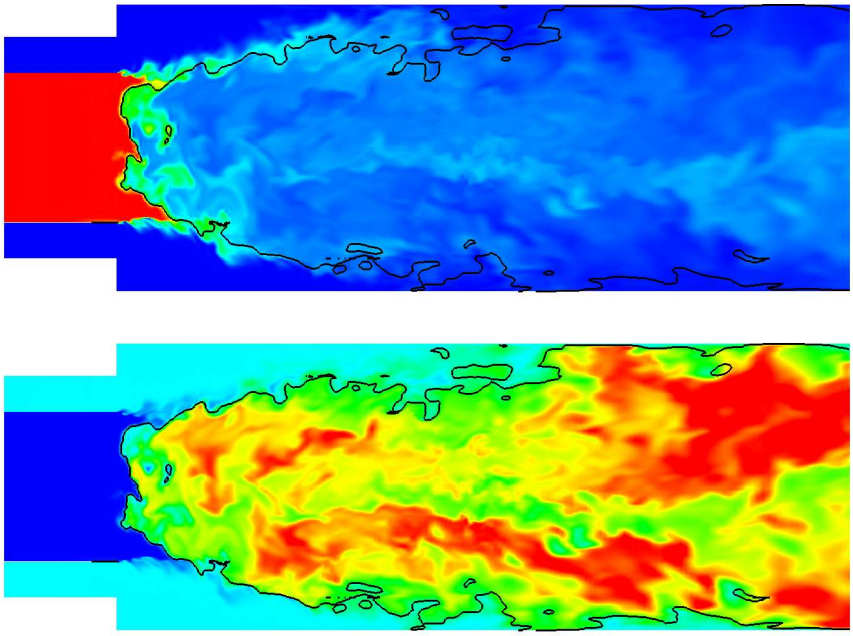

Figure 8: Contour plot of partially premixed dump combustor simulation. The black line represents the partially premixed interpretation of the flame front. With red denoting high and blue denoting low values, the quantities and ranges shown are, from top to bottom: (a) Mixture Fraction $[0, 1]$ (b) Temperature $[300, 2100]$ K.

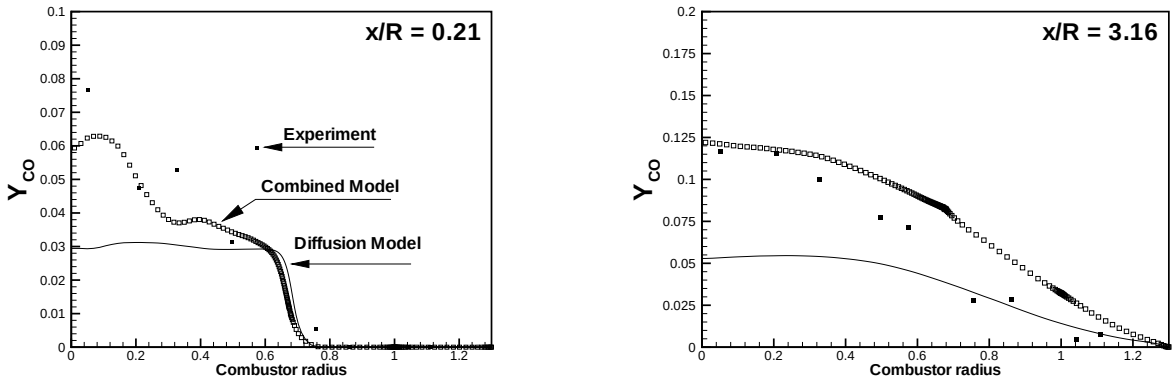

Figure 9: CO mass fractions predicted by a diffusion-only and a combined diffusion/level set model at two axial locations in the combustor.

2 Development of Reduced Kinetic Mechanisms for JP-8 and Transportation Surrogate Fuels

2.1 Introduction

For the application of LES in combustion simulations of real technical devices, the chemical details of the fuel have to be considered. Computations with detailed chemistry can be done,

for instance, for natural gas but become very complicated for the class of fuels typically used in transportation. Gasoline, diesel, and jet fuels are refined products of petroleum, or crude oil, and are mixtures of hundreds of different hydrocarbon species that meet a certain number of general physical specifications like minimum flash point or maximum freeze point temperatures, heat of combustion, boiling range, and volatility. Thus, there can be significant variations in fuel properties and compositions from various feedstocks and refining processes. Representative samples of these fuels, called reference fuels, are used in the industry to validate engine design and performance. However, it now is acknowledged widely that much simpler surrogate fuels should be used in laboratory experiments and computational simulations to improve reproducibility and fundamental understanding of the combustion processes.

Surrogate fuels are defined as mixtures of a limited number of hydrocarbon species that will have similar physical and/or chemical properties to those of the real fuels. Among the most important properties that might have to be matched are the heat release, which is essentially reflected in the C/H ratio, the density, the boiling range, the tendency to form pollutants such as NO_x and soot, burning velocities, and auto-ignition characteristics. Most of the hydrocarbons in transportation fuels are members of the four major classes of hydrocarbons: paraffins, aromatics, naphthenes, and olefins. Recently, six chemical classes have been isolated that are presumed to form the minimal set of constituent types necessary to describe the chemical composition of real fuels [19], namely iso-paraffins, normal paraffins, single ring aromatics, cyclo-paraffins, olefins, and multi-ring aromatics.

The selection of components for a surrogate fuel is controlled by its applications and accuracy requirements. The approach is first to define possible candidates for surrogate fuel ingredients. These candidates should be as close to the real fuel components as possible. However, the actual choice is restricted to those fuels for which either detailed chemical schemes exist, or fuels for which a fair amount of experimental data are available, and detailed mechanisms can be constructed with some confidence. A number of possible candidates belonging to the six chemical classes presented above have been proposed recently [19]. Iso-octane has been proposed as an iso-paraffin, n-heptane, n-hexadecane, and n-decane as normal paraffins, toluene and different xylenes as one-ring aromatics, methylcylcohexane as a cyclo-paraffin, 1-pentene as an olefin, and α-methylnaphthalene as a multi-ring aromatic.

Detailed mechanisms for some of the components have been developed by Curran et al. for iso-octane [20] and n-heptane [21], by Bikas and Peters [22] for n-decane, and by Pitsch for α-methylnaphthalene [23]. Also, semi-detailed and detailed mechanisms for certain mixtures have been provided. For example, a detailed mechanism for mixtures of iso-octane and n-heptane, the so-called primary reference fuel mixtures, has been developed by Curran et al. [24], and semi-detailed or lumped mechanisms of multi-component jet fuel surrogates have been proposed by Violi et al. [25] and Agosta et al. [26].

Several obstacles have to be overcome, however, to use these mechanisms as fuel surrogates in computational fluid dynamics (CFD) simulations. First, in constructing a multi-component surrogate fuel, several detailed mechanisms of individual components have to be combined. Experience shows that this combination is a formidable task. Another complication is the size

of most detailed mechanisms. Typically, the detailed mechanisms of single components have hundreds, or even nearly one thousand, species. A detailed mechanism for a multi-component surrogate will, consequently, also have perhaps five hundred to one thousand species. For most models presently used in LES, the maximum possible number of species is quite restricted. Steady flamelet models can tolerate up to hundreds of species, unsteady flamelet or CMC models perhaps fifty, and transported PDF models about fifteen to twenty. It is clear that chemical schemes for surrogate fuels cannot be used unless good reduced chemical mechanisms are available.

The top-down approach of first developing detailed mechanisms for individual components, combining these mechanisms, and performing the reduction is very time consuming and inflexible. For example, after adding a new component to the detailed mechanism, the reduction has to be redone. Also, the detailed mechanism has to include all reactions for auto-ignition and formation of pollutants, even though these reactions might not be required for every application.

To achieve more flexibility in the surrogate fuel modeling, we have proposed and demonstrated a different approach. Once the possible components of different surrogates are defined, validated detailed mechanisms for each of the individual components are identified. These detailed mechanisms are reduced independently for various conditions and accuracy requirements. The skeletal mechanisms form the so-called component library. Combining the corresponding elementary skeletal mechanisms for each component then creates a variety of chemical models for surrogate fuels. The skeletal mechanism for the multi-component surrogate then is validated through a comparison with experimental data. This approach makes it substantially easier to add a new component to a surrogate. The approach also greatly simplifies the merging of the mechanisms of the individual components, since this merging now is done at the level of the skeletal mechanism.

In the following section, the method first will be reviewed in detail, then an example will be provided, showing how this approach can be used to design a skeletal mechanism for a surrogate fuel.

2.2 Methodology

As mentioned above, detailed kinetic mechanisms are now available for a significant number of hydrocarbon fuels. However, these mechanisms usually are designed to model accurately fuel oxidation or auto-ignition over a large domain in temperature, pressure, and initial concentration space and can include thousands of reactions and up to one thousand species, which prohibits their direct implementation in flow simulations. Mechanism reduction aims to reduce those mechanisms to the smallest possible size that still leads to an accurate prediction of a number of chosen targets over the domain of interest. The first major step of a reduction process identifies all species and reactions that have little or no influence on the targets and removes them definitively from the mechanism. The number of differential equations that have to be solved is reduced by reducing the number of species and the computation of source terms is accelerated by removing unimportant reactions. This step reduces detailed mechanisms to the so-called skeletal level.

As most of the computational savings come from the reduction of the number of differential equations to be solved, it is essential to be able to identify species that do not play an important role during the chemical processes correctly. To gain insight into the complex chemical dynamics, Bendtsen et al. [27] introduced a reaction matrix $\underline{\underline{P}}$ defined at any time t, whose elements P_{ij} correspond to the production of species j from all reactions involving species i as a reactant at time t. This matrix quantifies the interactions existing between species and is used to select important species iteratively. The selection process starts with a set of major products or reactants. Species that contribute more than a certain percentage to the overall removal or production of any of these important species are included in the set. This procedure is repeated until no more species are included. The results were used to generate pathway plots at several times showing graphically the conversion of fuel into main intermediates and then into main products.

Tham et al. [28] used the same reaction matrix to select an initial pool of species: for each of the major products or reactants, an additional set of important species is selected by going through the reaction matrix following the path that connects one species to the next that is coupled most strongly with it. A second step selects, for each of those species, a subset of reactions such that a certain percentage of the total formation or destruction of that species is kept in the skeletal mechanism. Any additional species appearing in these reactions then are added to the list of important species, and this last step is repeated until no more species are added. Reactions involving large heat release also are added to the mechanism. No threshold is needed for the selection of the initial set of species. This method is efficient in selecting important reactions but tends to retain a large number of species for a given accuracy.

Recently, Lu et al. [29] used a species selection procedure similar to the one proposed by Bendtson et al. [27] but applied it to the automatic generation of skeletal mechanisms with various complexities and domains of applicability. Given a threshold parameter ϵ, a directed relation graph (DRG) is constructed, whose nodes correspond to species present in the mechanism. There exists a directed edge from species A to species B only if the normalized interaction coefficient r_{AB} that quantifies the dependence of species A on species B is greater than ϵ. The interaction coefficient is defined as

$$r_{AB} \equiv \frac{\sum_{i=1,I} |\nu_{A,i}\omega_i\delta_{Bi}|}{\sum_{i=1,I} |\nu_{A,i}\omega_i|}\,, \tag{14}$$

where the subscript i designates the i^{th} elementary reaction, $\nu_{A,i}$ the stoichiometric coefficient of species A in reaction i, ω_i the production rate of species A for the reaction i, and δ_{Bi} is the Kronecker symbol

$$\delta_{Bi} = \begin{cases} 1, & \text{if the i}^{\text{th}}\text{ reaction involves species B} \\ 0, & \text{otherwise} \end{cases}$$

If A is to be kept in the skeletal mechanism, then B has to be kept too. To initiate the selection process, the user must specify a set of starting species, which may be just a single species, namely the fuel. Species kept are those that are reachable from species included in the initial set.

This method was applied to auto-ignition and Perfectly Stirred Reactor (PSR) simulations. The pre-defined domain of applicability of the skeletal mechanism to be generated is densely sampled in pressure, equivalence ratio, temperature, and time. The DRG selection method is applied to each of those points, and the final resulting skeletal mechanism is the union of the sets of species obtained at each sample point. The selection process is fast, requires a single evaluation of the solution using the detailed mechanism, and depends on one unique user-defined parameter. However, a major drawback of this method is that the value of ϵ is not directly related to an error measure. One value for ϵ applied to different mechanisms will return disparate species reduction ratios and accuracies. Moreover, the DRG method assumes that every species selected is equally important and that the set of strongly coupled species associated with each important species has to be kept entirely, which may not be necessary. These issues are addressed in the following sections, where a modified version of the DRG method is proposed and evaluated.

2.2.1 Directed Relation Graph Method with Error Propagation [30]

For each species A present in a kinetic mechanism, a set of primary dependent species can be defined, consisting of those species that appear explicitly in reactions involving A. The strength of the interaction between A and species B of this primary dependent set is defined by the interaction coefficient r_{AB} defined in Eq. 14. A directed relation graph can be constructed as stated by Lu et al. [29] using $\epsilon = 0$. If species B is not in the primary dependent set of A, then $r_{AB} = 0$.

Species A will depend not only on the species contained in its primary dependent set, but also on all species directly related to its primary dependent set. However, species C interacting with species A through a third species B is important for A only if it is important for B and if B is important for A. To quantify this more complex coupling, we define a path-dependent coefficient $r_{AB,i}$ on path i from A to B as being the product of each primary interaction coefficient encountered on the path.

In Figure 10, for example, if path #1 is $A \rightarrow B \rightarrow D$, the coupling coefficient between A and D is

$$r_{AD,1} = r_{AB} \cdot r_{BD} \, .$$

If an error is made on D, it propagates through B and, the larger the coupling coefficient between A and D is, the larger the impact this error will have on A. Finally, we define the generalized interaction coefficient of species A with species B as the maximum path-dependent coefficient between A and B

$$R_{AB} \equiv \max_{\text{all paths i}} \{r_{AB,i}\} \, .$$

For example, in Figure 10, A depends on C

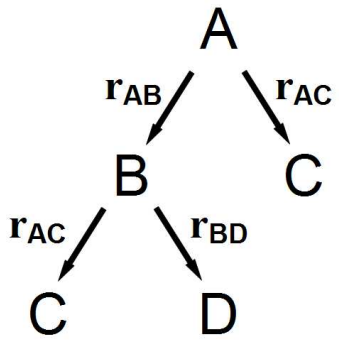

Figure 10: Interaction graph between four species; coefficients r correspond to primary interactions. Species A depends on species C and D through its interaction with species B

with coefficient

$$R_{AC} = \max\{r_{AB} \cdot r_{BC}, r_{AC}\} \ .$$

Each species is associated with a subset of species that is sorted in order of the coupling strength existing between them. For species A, a subset of the most important species with respect to some threshold value ϵ can be formed by keeping in the set only the species i for which

$$R_{AB} \geq \epsilon \, .$$

The smaller ϵ is, the more species are included in the set, so that species A can be predicted more accurately.

The skeletal mechanism corresponding to one particular value of ϵ then is generated as follows. First, a set of target species is defined. This set includes the species whose evolution should be described accurately by the skeletal mechanism, usually the major reactants and products, NO and NO_2 if we are interested in NO_x formation, and any additional species of special interest. By defining some threshold ϵ, a subset of important species for each of the targets is selected automatically following the procedure described above. The complete set of species to be kept is the union of all these subsets. Any elementary reaction containing a species that has not been selected is removed from the mechanism.

The major difference between this new selection method and the DRG theory is that it allows a finer selection of species since it focuses on how the error made on any single species will propagate to the targets. Selected species are not equally important anymore, as those species that are farther from the targets are comparatively more important for the species to which they are related than those directly linked to the targets. As a consequence, the choice of the targets must be made carefully since only the targets will be guaranteed to be described accurately. The level of accuracy of any other species will be determined by the target selection, and the agreement between the skeletal and detailed mechanism may be quite poor for those species. This discrepancy is not a problem as long as the user is aware of the conditions for which the skeletal mechanism has been developed.

An illustration of this species selection process is given in Figure 11. Species A is the target. Species B and D contribute 5% and 4%, respectively, to the production of target A. Species C has a 10% effect on species B. Computing the global coefficients for each species and rearranging, even if C had the largest direct interaction coefficient, it only has a small effect on the prediction of A, and, therefore, it should be removed first, whereas species D that had the smallest coefficient is kept in the reduced scheme.

The DRGEP method identifies unimportant species and removes them from the skeletal mechanism. The method insures that the most important steps, associated with the most important species are retained. The global coefficients do not distinguish between production and consumption of the species, as they involve the absolute values of the production and consumption rates. However, removing all the consumption reactions for a species can sometimes lead to a important concentration build-up for this species, introducing an error more important than what was predicted by the coefficient itself. An additional check on the production and consumption of each species is made during the selection process that keeps or removes extra species so as to avoid such build-up cases.

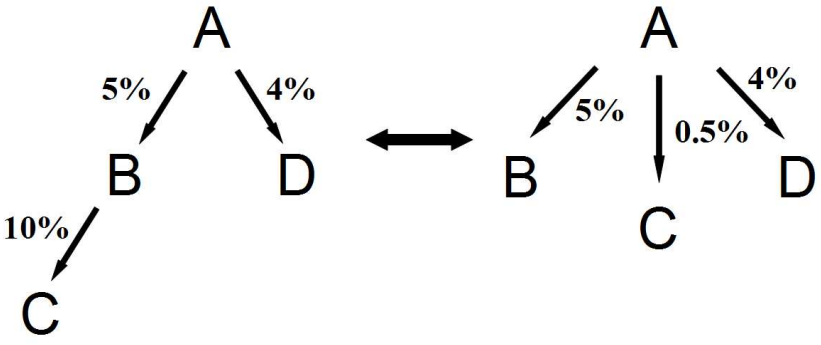

Figure 11: Example of species selection using DRGEP

Once unimportant species are identified, not every reaction step involving important species is important. A second level of reduction addresses this issue. If a step does not contribute significantly to the production or consumption rate of each species appearing in this reaction, it can be removed safely, provided that the overall production and consumption rates of each of those species remain close to the original ones. Assuming that the first step keeps all necessary species needed to reproduce the detailed mechanism results to a given accuracy, removing extra unimportant reactions should leave the number of species unchanged. The following procedure thus is applied to each species selected by the first step. Considering forward and backward reactions separately, normalized production and consumption rates of a species i with respect to a reaction j are defined by:

$$P_{ij} = \frac{|\max(0, \nu_{ij})\omega_j|}{\sum_k |\max(0, \nu_{ik})\omega_k|}\,,$$
$$C_{ij} = \frac{|\min(0, \nu_{ij})\omega_j|}{\sum_k |\min(0, \nu_{ik})\omega_k|}\,.$$

For each species i that has been retained, both the normalized production and consumption rates for each irreversible reaction involving that species are sorted by increasing value. For a given threshold δ, there exists an index J such that:

$$\frac{\sum_{j=1}^{J}(P_{ij})}{\sum_{\mathrm{all\ j}} P_{ij}} > \delta \;\text{ and }\; \frac{\sum_{\mathrm{j=1}}^{\mathrm{J}}(\mathrm{C_{ij}})}{\sum_{\mathrm{all\ j}} \mathrm{C_{ij}}} > \delta\,.$$

Only reactions from 1 to J are included in the subset of reactions. The final subset of reactions is the union of the subsets obtained for each species. The threshold δ either can be a global threshold or can depend on the interactions between the species and the targets, and hence on the propagation of errors.

2.2.2 Automatic Reduction Procedure

The previous section explained how a skeletal mechanism can be generated for a given ϵ and δ. This section addresses issues concerning the data used to select species and reactions, how to measure the error between skeletal and detailed mechanisms, and the iterative procedure followed to obtain the values of ϵ and δ that give the best reduction possible. This section also provides an overview of the whole reduction procedure from the perspective of a user.

Space Sampling Detailed mechanisms are generally valid over a much wider domain in pressure, temperature and concentration than needed in practical applications. A skeletal mechanism will be constructed to match the detailed one only over narrower well-defined regions. Several points that are characteristic of this restricted domain are selected on which the skeletal mechanism will be required to satisfy a certain accuracy. If those points are well-chosen, the reduced mechanism should remain valid inside the region mapped by them. These points can include auto-ignition of homogeneous systems, diffusion or premixed flames at various pressures, temperatures, and equivalence ratios.

Error Evaluation The most accurate way to evaluate the error introduced in the skeletal mechanism is to compute the solution using this skeletal mechanism and compare it to the solution obtained using the detailed mechanism. At each sample point, depending on the kind of simulation done, an error is computed for temperature, ignition delay time, laminar burning velocity, and concentrations of the targets, scaled to be between 0 and 1. The global errors are the maximum errors over all sample points, and each of them has to satisfy the corresponding user-defined accuracy requirement for the skeletal mechanism to be valid.

Iterative Process It has been shown that this method removes species so that the global error increases as the number of species decreases in a monotonic and relatively smooth way. Thus, the optimal skeletal mechanism can be obtained through a bisection search. Starting from two values of ϵ, the first one, $\epsilon_{\max}$, associated with an unacceptable error, the second one, $\epsilon_{\min}$, with an error within the tolerances, a new ϵ is chosen equidistant to $\epsilon_{\min}$ and $\epsilon_{\max}$ and the corresponding skeletal mechanism is constructed and evaluated. Depending on the quality of this new mechanism, either $\epsilon_{\min}$ or $\epsilon_{\max}$ is replaced by this new value, and the procedure is repeated until the best acceptable mechanism is found.

Even if the optimal value for ϵ is different from one mechanism to another, the order of magnitude usually remains the same. The initial boundary values for ϵ can be chosen accordingly, and the whole procedure converges in only a few iterations. Moreover, evaluating the solution on a skeletal mechanism is much cheaper than on the detailed one, and solutions for large values of ϵ are seldom evaluated entirely, as the skeletal mechanism is rejected as soon as the solution at one point exceeds the tolerated error.

2.2.3 User Input

The code has been written in Perl (Practical Extraction and Report Language) and is interfaced with the chemistry code FlameMaster [31]. Aside the kinetic mechanism and the thermodynamic and transport data for the species appearing in the mechanism, the user must provide an input file that includes the physical configurations for which the skeletal mechanism must

be valid, the target parameters for each case and the error tolerances. An example of input file is given in Figure 12. A skeletal mechanism that satisfies the error tolerances for each target and each case is generated automatically.

2.3 Examples

In this section each step that one must follow to generate a skeletal model for a surrogate fuel will be presented. The detailed kinetic mechanisms used for this example have been obtained from Lawrence Livermore National Laboratories. Taking all the mechanisms from a single source presents several advantages. First, the basic C_1-C_4 mechanism is identical for all mechanisms, which greatly simplifies the merging of the skeletal mechanisms of the individual components. This merging can be done, in general, for any type of mechanism, but then the validation steps become much more crucial and should be done with extra care. Also, the species nomenclature is fairly uniform, which avoids any duplicated species or reactions in the final combined mechanism. Finally, the thermodynamic and transport data are similar for each detailed mechanism. Those data are of primary importance in the determination of reaction rates, especially for reversible reactions. Using one set of thermodynamic data insures that the reaction rates in the combined mechanism will remain coherent. Those mechanisms have been validated against a large number of experimental data. Therefore, we can have confidence in the results obtained with them.

Although taking all the mechanisms from a single source introduces simplifications in the process, there is a major drawback: the detailed mechanisms currently available do not include fuels larger than iso-octane. Jet fuels have an average carbon number of 11, and appropriate surrogates would include large molecules such as dodecane or butyl-cyclohexane. On the other hand, molecules such as heptane, iso-octane, and toluene are appropriate for gasoline surrogates. A surrogate for gasoline was designed and studied experimentally by Gauthier et al. [32]. Its composition is given in Table 1. It will be used here as a test case to validate the method.

	vol%	mol%
Iso-octane	63.0	55.7
Heptane	17.0	16.9
Toluene	20.0	27.4

Table 1: Composition of Gasoline Surrogate.

The detailed mechanism for n-heptane [21] has 558 species, and the detailed mechanism for iso-octane [20] has 850 species. The toluene mechanism has been extracted from a mechanism for HCCI surrogate fuel by Pitz et al. [33] and consists of 321 species.

2.3.1 Validation of Detailed Mechanisms

Once the components of the surrogate are defined and appropriate detailed mechanisms have been identified, the next step is to validate those detailed mechanisms against experimental data. Because the mechanisms are extremely large, with hundreds of species, the only validation

```
# -------------------------- #
# GLOBAL CHEMISTRY PARAMETERS #
# -------------------------- #

Common {
  Mech:     ./gri.211.mech
  Thermo:   ./gri.211.thermo.bin
  Fuels:    CH4
  Oxidizer: O2
  Global Reaction:
         CH4 + 2O2 == CO2 + 2H2O
}

# -------- #
# 0D CASES #
# -------- #

Common0D {
  Restol:   1.0e-9
  Abstol:   1.0e-9
  Noutputs: 100
  Pressure: 1.0e5
}

Case0D {
  Flame:       isochor
  Temperature: 950/100/1350
  Composition: 0.5 1 2
  Targets:     Tig/0.1 CH4/0/0.1
}

Case0D {
  Flame:       isobar
  Temperature: 950
  Composition: 1
  Targets:     CH4/0/0.1 CO2/0/0.05
}
```

```
# -------- #
# 1D CASES #
# -------- #

Case1D {
  Flame:     Counterflow MixFrac
  TOxi:      400.0
  TFuel:     300.0
  VOxi:      -0.08745
  VFuel:     0.04821
  CompoOxi:  X->N2=0.8;X->O2=0.2;
  CompoFuel: X->CH4=0.49;X->N2=0.51
  Pressure:  1.0e5
  Targets:   T/0/0.1 CH4/1/0.2 O2/1/0.1
}


# -------------------- #
# REDUCTION PARAMETERS #
# -------------------- #

NAME:    debug
RECYCLE: 1 old_files
COMPARE: 0

SpecReduction {
  Type: standard
  Eval: Linear 2 Stop
}

ReacReduction {
  Type: KeepAllSpecs
  Eval: Bissection 0.9 1
}
```

Figure 12: Sample input file.

cases that can be done at this point are zero-dimensional, homogeneous configurations such as shock tube (ST) or Plug-Flow Reactor (PFR) experiments. Figure 13(a) shows comparisons between simulated ignition delay times and experimental data from Fieweger et al. [34] and from Gauthier et al. [32] for heptane. The simulation results match the experimental data well, but the mechanism tends to over-predict the ignition delay times at high temperatures. The mechanism for toluene had to be modified slightly to match experimental data for ignition times and species concentrations. Figure 13(b) compares the simulated time evolution of major species during the oxidation of toluene in a PFR with experimental data from Klotz et al. [35]. The agreement here is very good.

2.3.2 Reduction of the Detailed Mechanisms to a Skeletal Level

Each detailed mechanism is reduced independently to a skeletal level by using the DRGEP method. The reduction is performed for shock tube and PFR simulations over a wide range of initial conditions, and the maximum error tolerance is set to 10%. A comparison of the number of species before and after the reduction is shown in Table 2. The DRGEP method is very efficient at removing unimportant parts of the mechanism. Figure 14 shows a comparison between the skeletal mechanism obtained for n-heptane and the detailed mechanism. An error of 10% is actually reached at low temperatures, high temperatures, and around the NTC region.

Component	Detailed Mechanism	Skeletal Mechanism	Reduction ratio
Iso-octane	850	197	4.3
Heptane	558	170	3.3
Toluene	321	80	4.0

Table 2: Reduction of Detailed Mechanisms for the Individual Components.

2.3.3 Combination Step: Skeletal Mechanism for Gasoline Surrogates

A skeletal model for gasoline can be obtained by combining the individual skeletal mechanisms. The common parts of each mechanism are combined and the parts specific to the individual components are added automatically. The obtained mechanism for gasoline consists of 352 species. Figure 15 shows a comparison between the combined mechanism and experimental data by Fieweger et al. [34] obtained for mixtures of heptane and iso-octane. There is a very good agreement between the two mechanisms, showing that cross-reactions between iso-octane and heptane have little influence on the behavior of a mixture. Figure 16 compares ignition delay times obtained for the gasoline surrogate to experimental data by Gauthier et al. [32]. Although the simulated ignition times are over-predicted slightly, the overall agreement is fairly good.

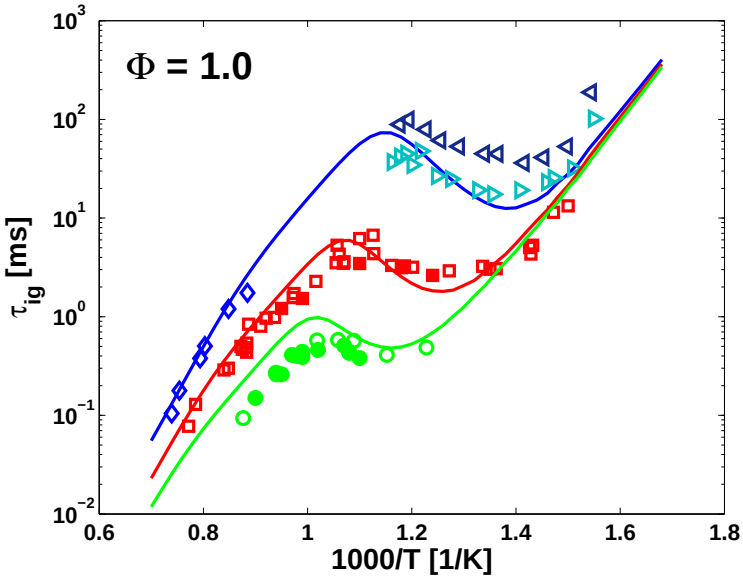

(a) Comparison of ignition delay times between LLNL n-heptane detailed mechanism (solid line) and experimental data by Fieweger et al. [34] (open symbols) and Gauthier et al. [32] (filled symbols).

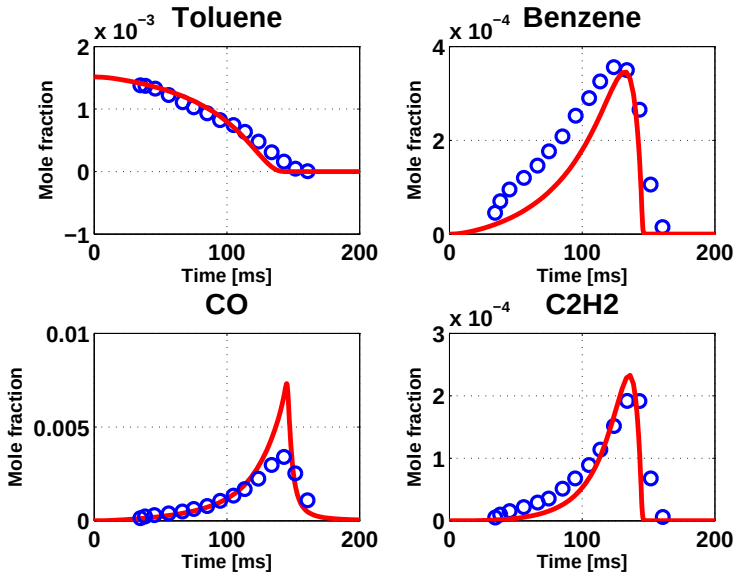

(b) Comparison of species concentrations in PFR between LLNL toluene detailed mechanism (solid line) and experimental data by Klotz et al. [35] (symbols).

Figure 13: Validation of detailed mechanisms for the individual components of a surrogate.

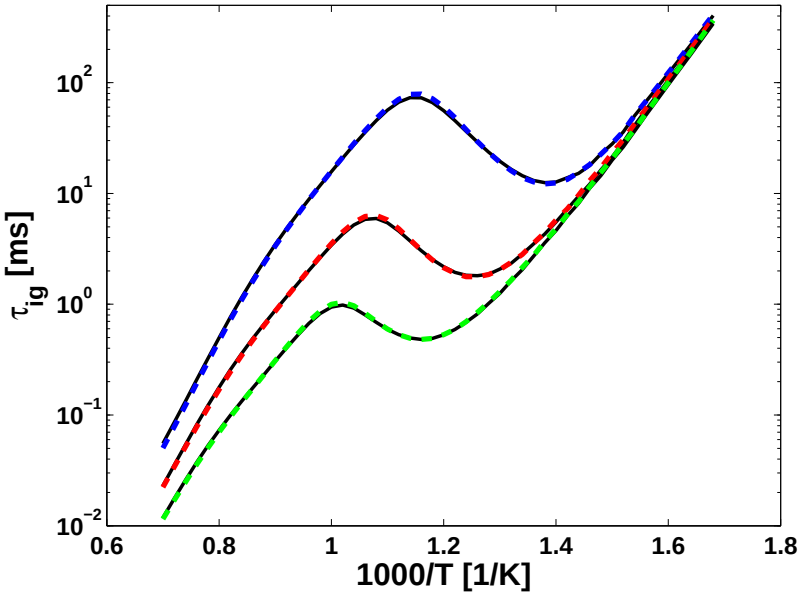

(a) Comparison of ignition delay times of skeletal mechanism (dashed line) compared with detailed mechanism (solid line) and .

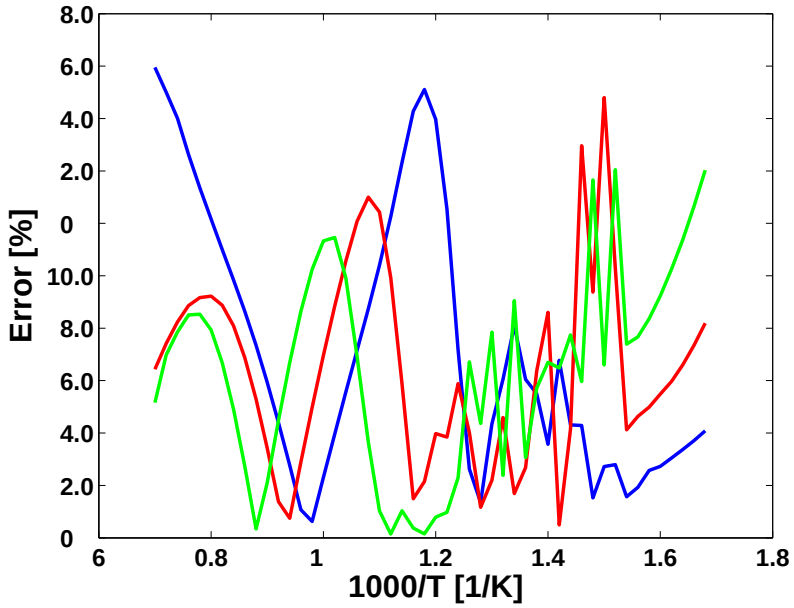

(b) Absolute value of error of skeletal mechanism compared with detailed mechanism.

Figure 14: Reduction of n-heptane mechanism - Stoichiometric ignition delay times for various pressures: p = 3.2 bar (blue line), p = 13.5 bar (red line) and p = 42 bar (green line).

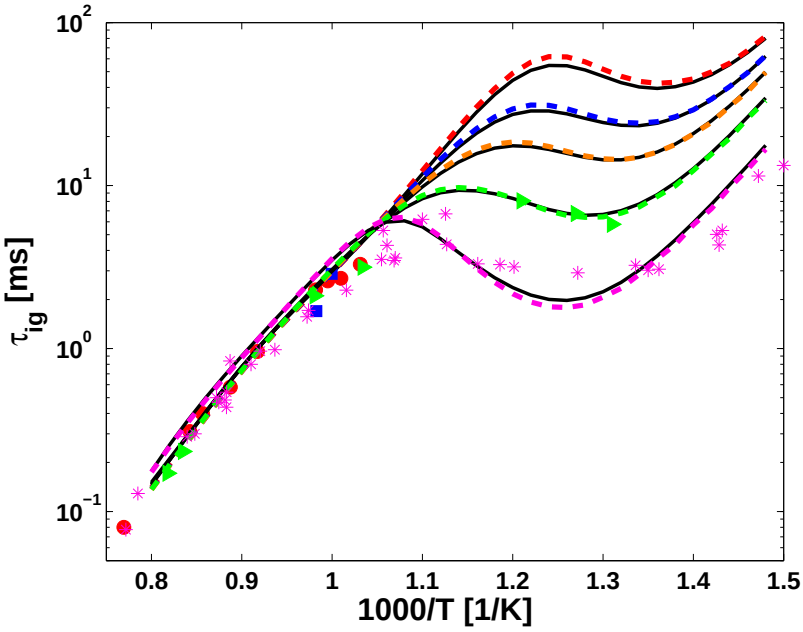

(a) Pressure = 13 bar

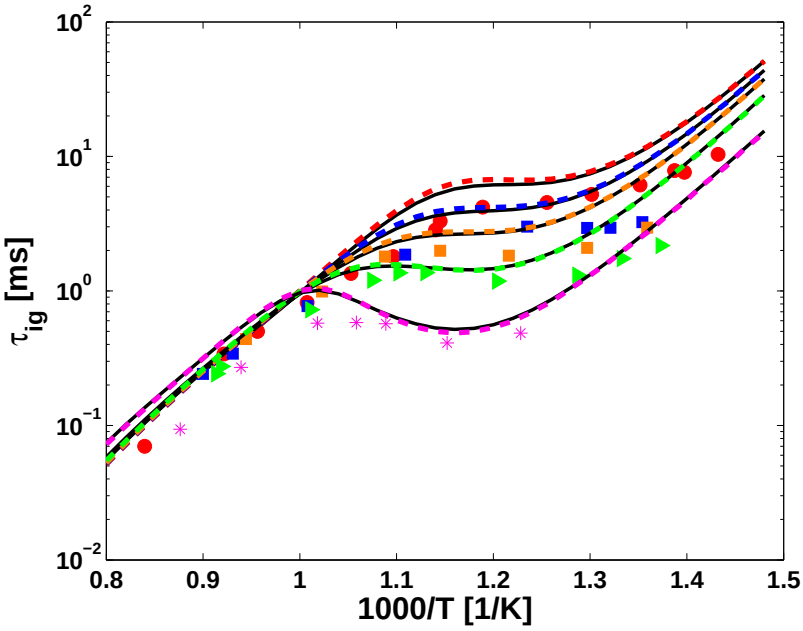

(b) Pressure = 40 bar

Figure 15: Reduction of primary reference fuels mechanism - Comparison of ignition delay times for various octane numbers: ON = 100 (red), ON = 90 (blue), ON = 80 (orange), ON = 60 (green), ON = 0 (magenta); detailed mechanism (black solid lines), skeletal mechanism obtained by automatic reduction (colored lined), experimental data (symbols).

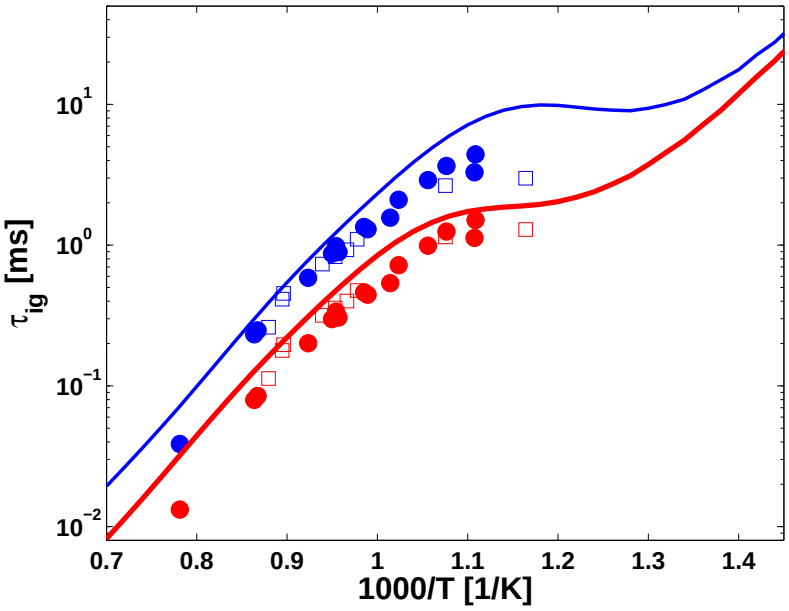

Figure 16: Gasoline ignition delay times - Comparison between simulations (solid line) and experimental data for gasoline (filled symbols) and gasoline surrogate (open symbols) at different pressures: p = 20 bar (blue line) and p = 55 bar (red line).

3 Conclusion

In the first part of this work, new models for describing sub-grid quantities in reactive LES settings were devised and validated. These models included a new model for the sub-filter variance of a conserved scalar, a new method of filtering the G-equation, a resolution sensitive description of the turbulent burning velocity, and a flamelet formulation valid near premixed fronts. The models have been shown to offer improved predictive capability through application to experimental flames. Furthermore, the new models have contributed to the identification of a significant sensitivity in premixed level set based models. Despite the development of these improved models, large eddy simulations still require accurate descriptions of chemistry from outside sources. Most often, these descriptions come from the solution of flamelet equations, which, in turn, require accurate, but computationally feasible, chemical mechanisms. This need motivates the second part of the work.

In that second part, a new method to automatically generate skeletal kinetic mechanisms for surrogate fuels, using the directed relation graph method with error propagation, has been proposed and evaluated. These mechanisms are guaranteed to match results obtained using detailed chemistry within a user-defined accuracy for any specified target. They can be combined together to produce adequate chemical models for surrogate fuels. A library containing skeletal mechanisms of various accuracies and domains of applicability has been assembled. New components will be added as corresponding validated detailed chemical mechanisms become available. However, the resulting combined mechanisms are too large to be used in practical CFD computation. They have to go through a second level of reduction that is currently under development. The strategies used in this second stage are different from those used to get the skeletal models and rely on automatic lumping of species and the use of Quasi-Steady State Assumptions to reduce the number of differential equations that have to be solved.

4 Participating personnel

During the reporting period, the PI and two graduate students, Perrine Pepiot and Dirk Veenema, have been supported within the present research grant.

5 List of Submitted and Accepted Publications in Reporting Period

5.1 Refereed Journal Publications

1. Pitsch, H., Large-Eddy Simulation of Turbulent Combustion, Ann. Rev. Fluid Mech., 38, pp. 453-483, 2006.

2. Pitsch, H., A Consistent Level Set Formulation for Large-Eddy Simulation of Premixed Turbulent Combustion, Comb. Flame, 143, pp. 587-598, 2005.

3. Raman, V., Pitsch, H., Large-Eddy Simulation of a Bluff-Body Stabilized Flame Using a Recursive-Refinement Procedure, Comb. Flame, 142, pp. 329-347, 2005.

6 Interactions and Transitions

6.1 Selected Presentations at Conferences and Seminars

1. Pitsch, H., Large-Eddy Simulation of Turbulent Combustion, Air Force Research Laboratories, October 2005

2. First Workshop on Quality Assessment of Unsteady Methods for Turbulent Combustion Prediction and Validation, Frankfurt, Germany, "Validation and Verification in LES of Reactive Flows", June 2005

3. Pepiot, P., Pitsch, H., Systematic Reduction of Large Chemical Mechanisms, 4th Joint Meeting of the U.S. Sections of the Combustion Institute, Philadelphia, PA, March 2005.

4. Workshop on Front Propagation and Nonlinear Stochastic PDEs for Combustion and other Applications, Montreal, "Level Set Methods in Large-Eddy Simulations of Premixed Turbulent Combustion", January 2005

6.2 Transitions

In the last year we have worked with scientists from AFRL to make different computer codes available to AFRL. We have discussed the transition of the software used for automatic reduction with the group of Dr. Zelina. Additionally, we are in the process of transferring the multi-physics unstructured LES code CDP to AFRL. The contact people at AFRL for this effort are Dr. Sekar and Dr. Zelina.

7 Patents and Inventions

None

References

[1] H. Pitsch and H. Steiner. Large-eddy simulation of a turbulent piloted methane/air diffusion flame (Sandia flame D). *Phys. Fluids*, 12(10):2541–2554, 2000.

[2] H. Pitsch. Improved pollutant predictions in large-eddy simulations of turbulent nonpremixed combustion by considering scalar dissipation rate fluctuations. *Proc. Combust. Inst.*, 29:1971–1978, 2002.

[3] H. Pitsch and L. Duchamp de Lageneste. Large-eddy simulation of premixed turbulent combustion using a level-set approach. *Proc. Combust. Inst.*, 29:2001–2008, 2002.

[4] H. Pitsch, M. Chen, and N. Peters. Unsteady flamelet modeling of turbulent hydrogen/air diffusion flames. *Proc. Combust. Inst.*, 27:1057–1064, 1998.

[5] L. K. Sua, O. S. Suna, and M. G. Mungal. Experimental investigation of stabilization mechanisms in turbulent, lifted jet diffusion flames. *Comb. Flame*, 144:494–512, 2006.

[6] D. Han and M. G. Mungal. Stabilization in turbulent lifted deflected-jet flames. *Proc. Combust. Inst.*, 29:1889–1895, 2002.

[7] A. W. Cook and J. J. Riley. A subgrid model for equilibrium chemistry in turbulent flows. *Phys. Fluids*, 6:2868–2870, 1994.

[8] C. D. Pierce and P. Moin. A dynamic model for subgrid-scale variance and dissipation rate of a conserved scalar. *Phys. Fluids*, 10:3041–3044, 1998.

[9] C. Jiménez, F. Ducros, B. Cuenot, and B. Bédat. Subgrid scale variance and dissipation of a scalar field in large eddy simulations. *Phys. Fluids*, 13(6):1748–1754, 2001.

[10] S.B. Pope. Ten questions concerning the large-eddy simulation of turbulent flows. *New Journal of Physics*, 6:35, 2004.

[11] V. Raman and H. Pitsch. Large-eddy simulation of a bluff-body stabilized flame using a recursive-refinement procedure. *Comb. Flame*, 142:329–347, 2005.

[12] B. B. Dally, A. R. Masri, R. S. Barlow, and G. J. Fietchner. Instantaneous and mean compositional structure of bluff-body stabilized nonpremixed flames. *Comb. Flame*, 114:119–148, 1998.

[13] F. A. Williams. Turbulent combustion. In J. D. Buckmaster, editor, *The Mathematics of Combustion*, pages 197–1318. Society for Industrial & Applied Mathematics, 1985.

[14] H. Pitsch. A consistent level set formulation for large-eddy simulation of premixed turbulent combustion. *Comb. Flame*, 143:587–598, 2005.

[15] Y. C. Chen, M. S. Mansour, and N. Peters. Measurements of the Detailed flame structure in turbulent H_2-air jet diffusion flames with line-raman/rayleigh/lipf-oh technique. *Proc. Combust. Inst.*, 26:97, 1996.

[16] N. Peters. *Turbulent Combustion*. Cambridge University Press, 2000.

[17] H. Pitsch, P. Trouillet, C. D. Pierce, E. Tribbett, C. M. Sipperley, C. F. Edwards, and C. T. Bowman. A joint experimental/large-eddy simulation study of a model gas turbine combustor. *Western States Section Meeting of the Combustion Institute, 2002, San Diego, CA*, pages WSSCI 02S–59, 2002.

[18] L. J. Spadaccini, F. K. Owen, and C. T. Bowman. Influence of aerodynamic phenomena on pollutant formation in combustion. EPA-600/2-76-247a, 1976.

[19] Workshop on Combustion Simulation Databases for Real Transportation Fuels. *National Institute of Standards and Technology, Gaithersburg, Maryland*, September 2003.

[20] H. J. Curran, P. Gaffuri, W. J. Pitz, and C. K. Westbrook. A comprehensive modeling study of iso-octane oxidation. *Comb. Flame*, 129:253–280, 2002.

[21] H. J. Curran, P. Gaffuri, W. J. Pitz, and C. K. Westbrook. A comprehensive modeling study of n-heptane oxidation. *Comb. Flame*, 114:149–177, 1998.

[22] G. Bikas and N. Peters. Kinetic modelling of n-decane combustion and autoignition - modeling combustion of n-decane. *Comb. Flame*, 114:1456–1475, 2001.

[23] H. Pitsch. Detailed kinetic reaction mechanism for ignition and oxidation of α-methylnaphthalene. *Proc. Combust. Inst.*, 26:721–728, 1996.

[24] H. J. Curran, W. J. Pitz, C. K. Westbrook, C. V. Callahan, and F. L. Dryer. Oxidation of automotive primary reference fuels at elevated pressures. *Proc. Comb. Inst.*, 27:379–387, 1998.

[25] A. Violi, S. Yan, E. G. Eddings, A. F. Sarofim, S. Granata, T. Faravelli, and E. Ranzi. Experimental formulation and kinetic model for jp-8 surrogate mixtures. *Comb. Sci. Tech.*, 174:399–417, 2002.

[26] A. Agosta, D. B. Lenhert, D. L. Miller, and N. P Cernansky. Development and evaluation of a jp-8 surrogate that models preignition behavior in a pressurized flow reactor. *3*$^{\text{nd}}$ *Joint meeting of the US sections of the Combustion Institute, Chicago, OH*, page paper E07, 2003.

[27] A.B. Bendtsen, P. Glarborg, and K. Dam-Johansen. Visualization methods in analysis of detailed chemical kinetics modelling. *Computers and Chemistry*, 25:161–170, 2001.

[28] Y.F. Tham and J.Y. Chen. Recent advancement on automatic generation of simplified mechanisms. *Western States Section - Combustion Institute*, 2003.

[29] T. Lu and C.K. Law. A Directed Relation Graph Method for Mechanism Reduction. *Proc. Comb. Inst.*, 30, 2005.

[30] P. Pepiot and H. Pitsch. Systematic Reduction of Large Chemical Kinetic Mechanisms. *Proceedings of the 4th Joint Meeting of the U.S. Sections of the Combustion Institute*, 2005.

[31] H. Pitsch. *A C++ Computer Program for 0D Combustion and 1D Laminar Flame Calculations.*

[32] B.M. Gauthier, D.F. Davidson, and R.K. Hanson. Shock tube determination of ignition delay times in full-blend and surrogate fuel mixtures. *Comb. Flame*, 139:300–311, 2004.

[33] C.V. Naik, W.J. Pitz, M. Sjoberg, J.E. Dec, J. Orme, H.J. Curran, J.M. Simmie, and C.K. Westbrook. Detailed Chemical Kinetic Modeling of Surrogate Fuels for Gasoline and Application to an HCCI Engine. *Proceedings of the 4th Joint Meeting of the U.S. Sections of the Combustion Institute*, 2005.

[34] K. Fieweger. *Selbstzündung von Kohlenwasserstoff/Luft-Gemischen unter motorischen Randbedingungen*. PhD thesis, RWTH Aachen, 1996.

[35] S. D. Klotz, K. Brezinsky, and I. Glassman. Modeling the combustion of toluene-butane blends. *Proc. Combust. Inst.*, 27:337–344, 1998.